Stress intensity factors of embedded elliptical cracks and an assessment of the ASME XI defect recharacterisation criteria

H. Noguchi

Faculty of Engineering, Kyushu University, 6-10-1 Hakozaki, Fukuoka 812, Japan

R. A. Smith,* J. J. Carruthers

Department of Mechanical and Process Engineering, University of Sheffield, Mappin Street, Sheffield S1 3JD, UK

&

M. D. Gilchrist

Mechanical Engineering Department, University College Dublin, Belfield, Dublin 4, Ireland

This paper considers aspects related to the calculation of the stress intensity factors of planar embedded defects in a solid under tension. The determination of stress intensity factor solutions using a modified body force method is described, this technique having certain advantages over existing finite element, boundary element and ordinary body force methods. Furthermore, comprehensive modified body force solutions are presented and discussed for a range of elliptical defect geometries.

These solutions have then been used to assess the conservation of the recharacterisation procedure for defects of complex geometry described in Section XI of the ASME Boiler and Pressure Vessel Code. Maximum stress intensity factor values calculated using both the modified body force method and the ASME XI rules in conjunction with standard solutions are compared and contrasted. The results of this analysis show that, by and large, ASME XI is conservative and hence safe. However, geometries for which ASME XI provides non-conservative estimates have been encountered and, in certain circumstances, this may be a cause for concern.

NOMENCLATURE

a, b	Lengths of half-major and half-minor axes of elliptical crack
a^*, b^*	Half-length and half-breadth of rectangle surrounding elliptical crack
a_{rech}, b_{rech}	Lengths of half-major and half-minor axes of recharacterised elliptical crack
R	Representative crack length
d	Perpendicular distance from the surface of the solid to the centre of the elliptical crack
E	Young's modulus
K_I	Mode I stress intensity factor at a point on the crack front
$K_{I,max}$	Maximum mode I stress intensity factor for a given crack front
s	Shortest perpendicular distance from the surface of the solid to the crack front
$W(\xi, \eta)$	Weighting function
W_f	Values of the weighting function on the crack front
α	Angle of rotation of the major/minor axes of the elliptical crack from the parallel/perpendicular to the surface of the solid
β	parametric angle defining a location on the crack front

* To whom correspondence should be addressed.

δ	Crack opening displacement
ε	Shortest distance from the point (ξ, η) to the crack front
ν	Poisson's ratio
σ_0	Tensile stress acting on the solid
ξ, η	Cartesian co-ordinates

1 INTRODUCTION

The accurate assessment of the significance of defects upon the safety, life and stability of engineering structures is of great importance. In performing such analyses designers commonly use a wide range of experimental, empirical and analytical stress intensity factor solutions which have been produced for idealised geometries. With this in mind, the objectives of this paper are twofold.

Firstly, an important series of Mode I stress intensity factor solutions are introduced. These have been developed using a modified body force method. Solutions are presented and discussed for embedded planar elliptical cracks in a solid under tension.

Secondly, an aspect related to the practical application of theoretical solutions for elliptical geometries is considered. Clearly, if such solutions are to be utilised for real-life defects, then some sort of recharacterisation procedure must be employed to translate the complex geometry of an actual crack into a representative ellipse. Section XI[1] of the ASME Boiler and Pressure Vessel Code provides a set of directions for doing this. However, it is not clear if the stress intensity factor values obtained for the ASME XI recharacterised defects are in agreement with those of the actual cracks being modelled. It is important to establish whether there is a significant discrepancy between the limiting stress intensity factor values for the actual cracks and their recharacterised counterparts. It is tacitly assumed that ASME XI will provide some degree of conservatism. An analysis which investigated this assumption is presented in the second half of this paper.

2 STRESS INTENSITY FACTOR SOLUTIONS

The modified body force method was introduced in earlier papers[2,3] as a technique for the analysis of surface or embedded plane cracks of arbitrary shape in a semi-infinite solid under complex loading conditions. Although the theory is based on the body force (or eigen strain) method,[4] it incorporates important improvements so that highly accurate numerical results are obtained even when coarse meshes are employed. In certain aspects the method is superior to the finite element method, the boundary element method and the ordinary body force method:

(1) it requires less input data than the finite element method because it is only necessary to discretise the crack plane;
(2) it is applicable to a wider range of crack shapes and loading conditions than the ordinary body force method;
(3) the numerical results are more accurate, even with coarse meshes, than the other methods;
(4) it is computationally less intensive than the other methods.

Explained briefly, the modified body force method takes Mindlin's[5] solution as a fundamental starting point and this is differentiated to obtain the stress field due to a point discrepancy or eigen strain. By considering the eigen value near the crack tip, the following expression for the crack opening displacement (COD), δ, is assumed:

$$\delta = \frac{4(1+\nu)}{E}\sqrt{2c\varepsilon - \varepsilon^2}\, W(\xi - \eta) \tag{1}$$

In eqn (1), ε is the shortest distance from the point (ξ, η) to the crack front, c is a representative crack length and $W(\xi, \eta)$ is a weighting function.

The crack is discretised using triangular elements and $W(\xi, \eta)$ is assumed to be a continuous function (Fig. 1). The boundary conditions are expressed in terms of the resultant forces, although, because of this, the triangular elements must be transformed into polygons (Fig. 2) in order to give an equal number of relationships and unknowns. The expression for the influence coefficient can then be obtained in analytical closed form.

Having replaced the boundary conditions on the crack front with the resultant force conditions, the value of the weighting function at each nodal point on the crack front, W_f, can be obtained by solving the resulting simultaneous linear equations. Having determined the value of W_f, the stress intensity factor is then given by:

$$K_I = W_f\sqrt{\pi c} \tag{2}$$

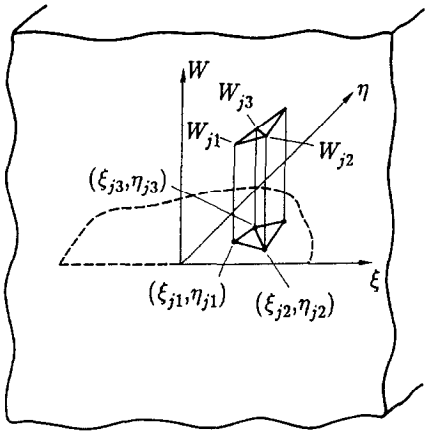

Fig. 1. Employed pattern of weighting function $W(\xi, \eta)$.

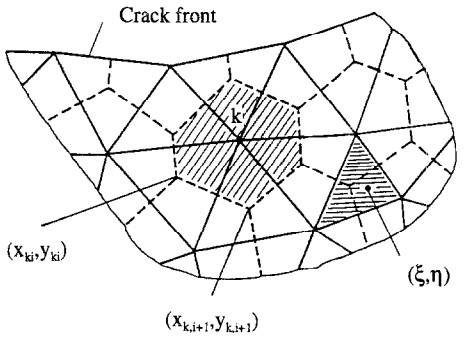

Fig. 2. Polygonal regions for the resultant force boundary conditions.

In this paper, the modified body force technique has been applied to three examples of single planar embedded elliptical cracks in a solid under tension. These are illustrated in Fig. 3. The major and minor axes of crack type A are aligned, respectively, parallel and perpendicular to the surface of the solid and the variation of stress intensity factor with the distance, d, of the centre of the crack from the surface of the solid has been examined. With crack type B, this distance has been fixed and instead the angle of rotation, α, of the major and minor axes relative to the surface of the solid has been varied. This is also the case with crack type C, although the major and minor axes have been interchanged relative to the solid's surface. In all cases, Poisson's ratio is taken as 0·3.

Figure 4 and Table 1 show the results of this analysis for crack types A, B and C as their position relative to the surface of the solid is varied. More comprehensive data, giving numerical values for the normalised stress intensity factor around the whole of the crack front, is included in the Appendix.

The validity of the solutions obtained using the modified body force method can be assessed by comparing them with results calculated by other authors. Mayrhofer & Fischer[6] used a semi-analytical procedure to calculate stress intensity factors for elliptical cracks similar to the ones discussed above. The modified body force technique has been applied to the same cracks investigated by Mayrhofer & Fischer and a comparison between the two methods is shown in Fig. 5. The non-dimensional ordinate, M, is the ratio of the stress intensity factor of the crack to that of a deeply buried ellipse. It can be seen that

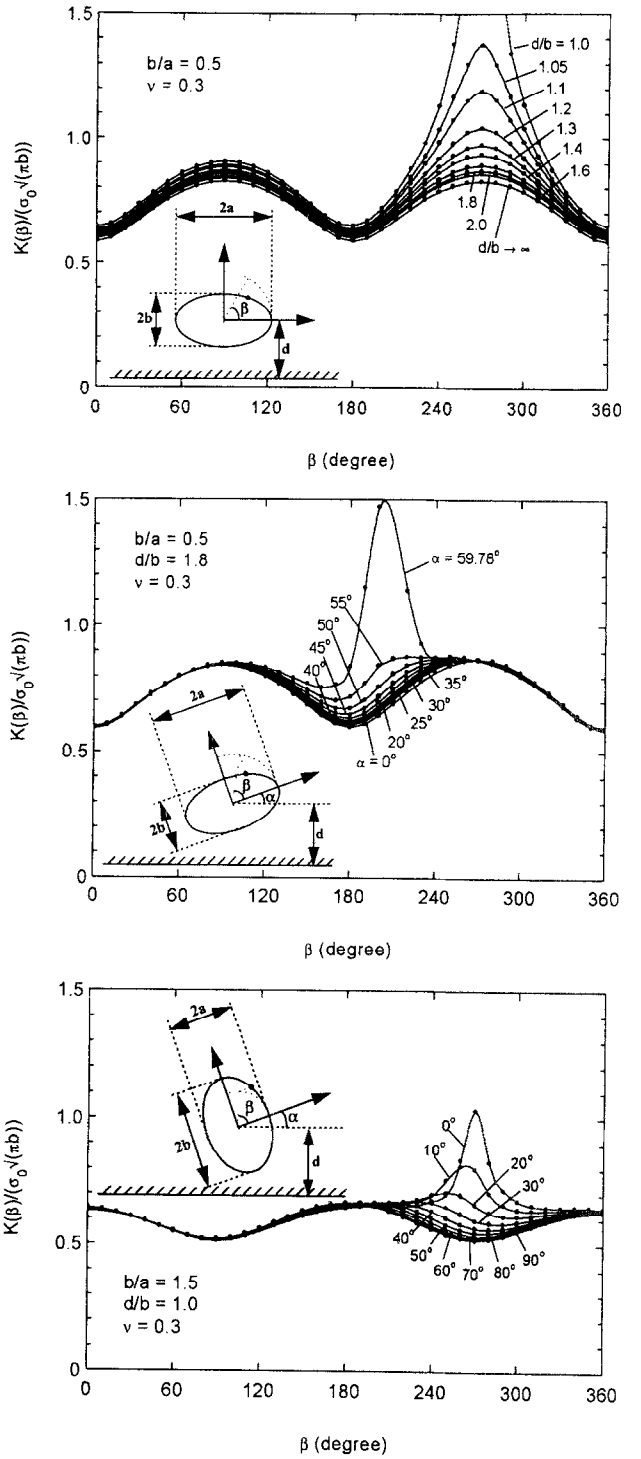

Fig. 4. Variation of the normalised stress intensity factor around the crack fronts.

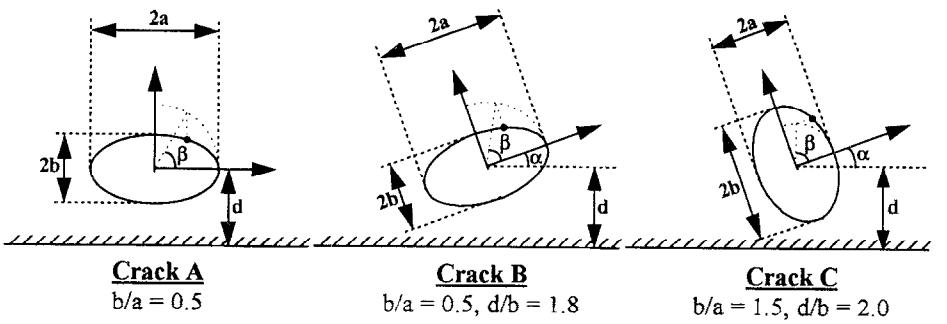

Fig. 3. Crack geometries for which solutions are presented.

Table 1. Magnitudes and locations of the normalised maximum stress intensity factor for crack types A, B and C

d/b	Crack A		α	Crack B		α	Crack C	
	Maximum $\frac{K_I}{\sigma_0\sqrt{\pi b}}$			Maximum $\frac{K_I}{\sigma_0\sqrt{\pi b}}$			Maximum $\frac{K_I}{\sigma_0\sqrt{\pi b}}$	
	Magnitude	*Position, β*		Magnitude	Position, β		Magnitude	Position, β
1·0	2·352	270°	0°	0·868	270°	0°	1·031	271°
1·05	1·373	270°	5°	0·868	269°	10°	0·817	264°
1·1	1·189	270°	10°	0·868	267°	20°	0·709	251°
1·2	1·040	270°	20°	0·868	265°	30°	0·672	228°
1·3	0·972	270°	25°	0·869	263°	45°	0·668	207°
1·4	0·933	270°	30°	0·870	261°	50°	0·667	200°
1·6	0·890	270°	35°	0·871	260°	60°	0·666	194°
1·8	0·868	270°	40°	0·871	257°	70°	0·666	189°
2·0	0·855	270°	45°	0·873	255°	80°	0·665	184°
∞	0·826	270°	50°	0·875	251°	90°	0·665	180°
			55°	0·878	240°			

there is generally very close agreement around the whole of the crack front for a variety of different geometries. Furthermore, for a deeply buried ellipse with major axis parallel to the free surface (crack type A, $d/b = \infty$) the normalised stress intensity factor of 0·826 at the ends of the minor axes ($\alpha = 90°$ and 270°) compares favourably with Shah and Kobayashi's[7] analytic solution of 0·828.

Finally, it would be worthwhile to conclude this section with some examples of design implications which arise from these solutions. The results for crack A demonstrate the considerable dependence of the stress intensity factor on the proximity of the crack to the solid's surface. Indeed, at a d/b ratio of 1·05, the maximum stress intensity factor is shown to be 66% larger than the value for a deeply buried crack. However, it can be seen that this surface magnification effect falls off quite sharply, with stress intensity factors only 26% and 8% larger than the deeply buried value at d/b ratios of 1·2 and 1·6 respectively. At d/b ratios greater than this, the effect of the solid's surface on the stress intensity factor can probably be considered to be negligible. These observations are, of course, similar to the approach effect of two parallel elliptical cracks remote from a free surface—see, for example, Isida *et al.*[8]

3 ASME XI DEFECT RECHARACTERISATION PROCEDURE

In undertaking the assessment of the structural significance of a crack-like defect, an engineer must know, amongst other things, geometric details of the crack under consideration. Since the geometries of real-life defects are likely to be complex, it is almost

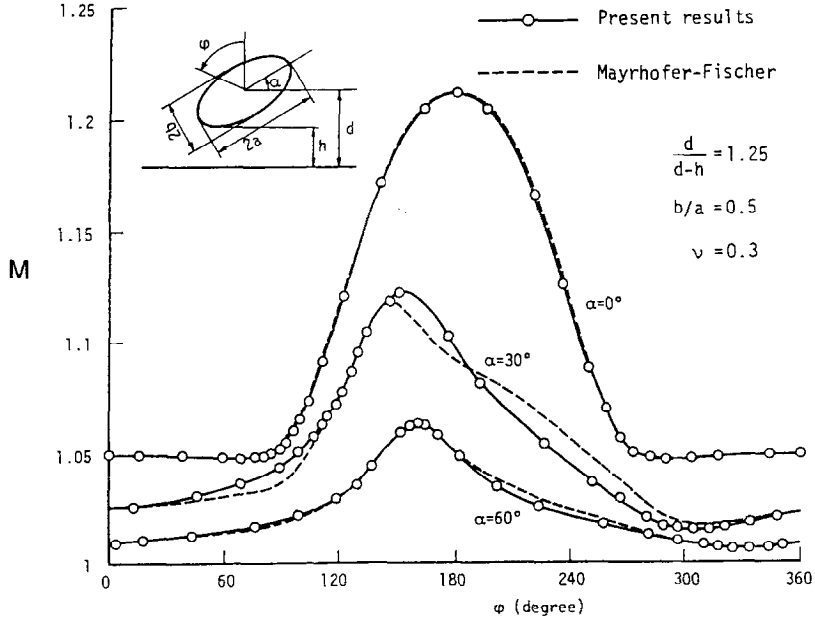

Fig. 5. Comparison of stress intensity values calculated by the present technique and by Mayrhofer & Fischer.[6] (The magnification ratio, M, is defined in the text; note that the angular position ϕ differs from β.)

inevitable that some sort of simplification procedure will be necessary in order to make the calculation viable. Section XI of the ASME Boiler and Pressure Vessel Code provides a series of directions for recharacterising the geometries of a wide range of defects into simpler forms which facilitate easy analysis. Single and multiple defects, planar and non-planar defects, and surface and embedded defects are all encompassed within ASME XI. Having recharacterised the defects into a more manageable form, engineers can then employ established solutions for the simplified geometry to obtain stress intensity factor estimates. However, as already explained, an assessment of the accuracy of modelling actual defects as ASME XI recharacterised cracks would be desirable. Therefore, the following analysis was undertaken.

The ellipses described in the previous section, for which accurate solutions have been provided, were recharacterised in accordance with the ASME rules. The stress intensity factors of these recharacterised ellipses were then calculated using standard solutions.[7,9] Comparing the stress intensity factors of the recharacterised ellipses with the modified body force method solutions for the actual ellipses provided an assessment of the conservatism of the recharacterisation procedure. Although the stress intensity factor varies around the crack front, it was only necessary to compare the maximum values since these are the critical criteria which determine defect growth and fatigue lives.

A flow chart of the recharacterisation procedure is shown in Fig. 6. The procedure basically involves enclosing the defect in a rectangle whose sides are parallel and perpendicular to the surface of the solid. The dimensions of this rectangle and its proximity to the solid's surface then dictate whether the recharacterised defect is considered to be embedded (elliptical) or surface-breaking (semi-elliptical). This

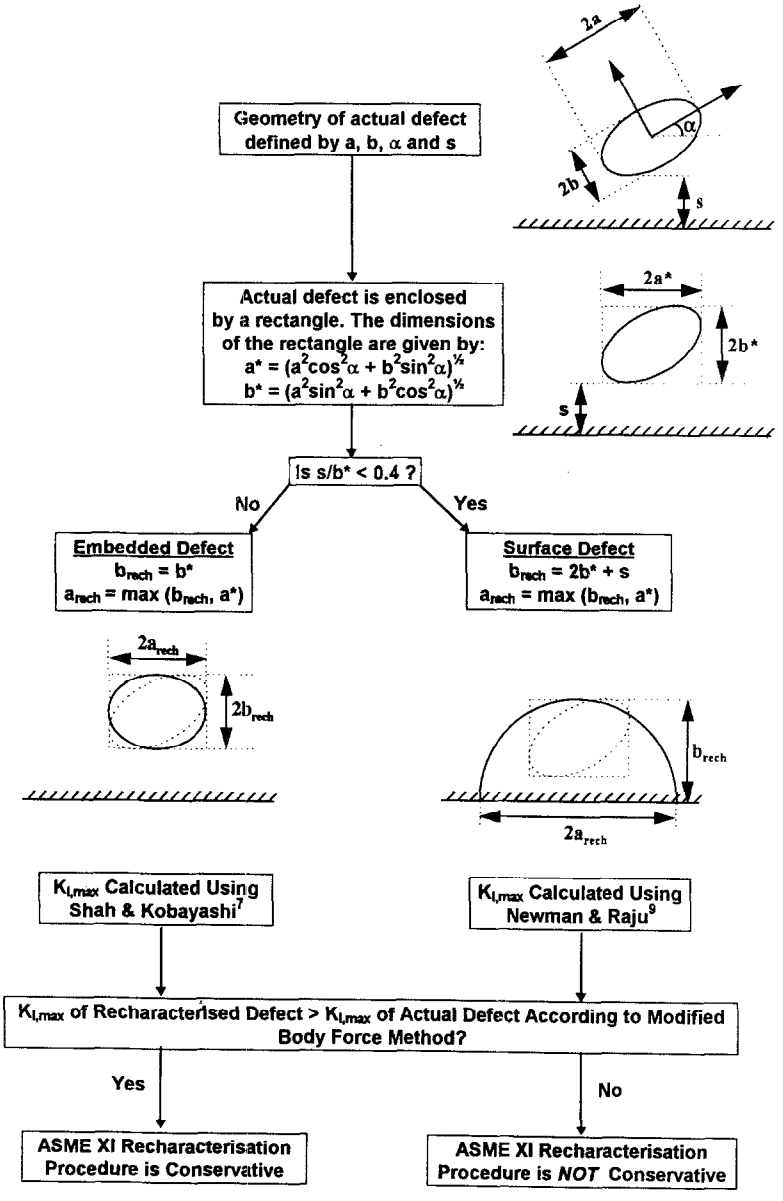

Fig. 6. Procedure for the recharacterisation of the defects and assessing the conservatism of ASME XI.

established, the geometry of the recharacterised defect can be calculated according to the rules in Fig. 6. In our work, Newman and Raju's[9] formula was used to calculate the maximum stress intensity factor of surface breaking defects, whilst that of Shah and Kobayashi[7] was employed for embedded flaws.

4 CONSERVATISM OF THE RECHARACTERISATION PROCEDURE

Figure 7 depicts the results of the conservatism analysis for crack types A, B and C. The ratio of the normalised modified body force method stress intensity factor to that of the ASME XI recharacterised crack is plotted on the ordinate and the geometric variable for the given crack is plotted on the abscissa. Consequently, ordinate values greater than one represent non-conservative recharacterisations. Each graph also indicates which geometries are recharacterised as being embedded flaws and which as surface breaking.

It can be seen that crack types A, B and C show the same general features. Those geometries which are recharacterised as embedded defects provide very accurate estimates of stress intensity factor with discrepancies as small as 5% or less. Surface breaking defects show a wide spread of results, although for the most part they tend to be conservative and hence safe.

However, given that Fig. 7 shows that there can be circumstances in which the application of ASME XI leads to non-conservative estimates of stress intensity factor, the possible implications of this should be considered. If the crack leads to a sudden, unstable mode of failure in a material with little or no crack-arrest capability, then any underestimation of the stress intensity factor could be disastrous. These are the situations in which the most caution should be exercised. However, it is also possible that the mode of failure will be a quasi-stable type of crack growth such as fatigue which will adjust the crack shape to equalise the stress intensity factor values around the periphery of the crack as the crack develops. This type of behaviour has been theoretically modelled and discussed in, for example, Gilchrist *et al.*[10] Therefore, in circumstances such as these, ASME XI's apparent lack of conservatism may be somewhat misleading. Clearly, knowledge of the failure mode is desirable if unnecessary rejection of a structure is to be avoided.

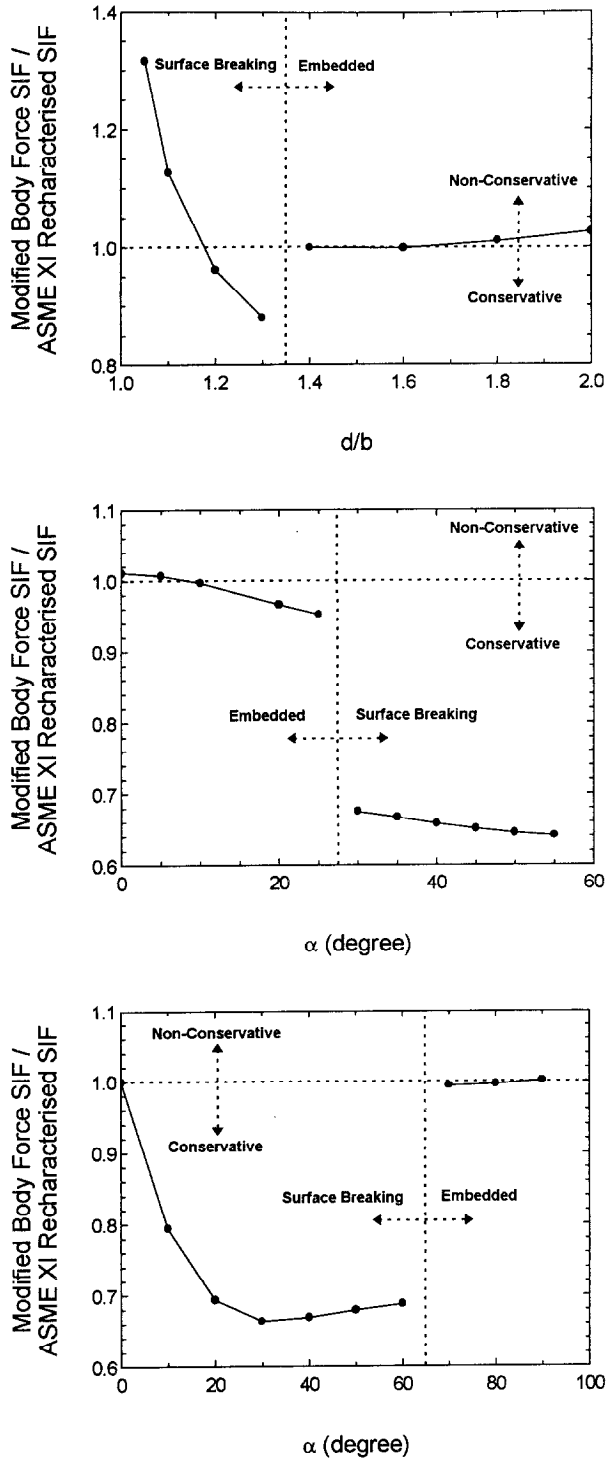

Fig. 7. ASME XI conservatism analysis for crack types A, B and C.

5 CONCLUSIONS

The modified body force method for the analysis of defects in a solid under complex loading conditions has been briefly described and applied to three types of embedded planar elliptical cracks. The resulting solutions for the stress intensity factors have then been used to demonstrate that whilst the recharacterisation process described in Section XI of the ASME Boiler and Pressure Vessel Code is for the most part conservative, there can be circumstances in which it leads to under-estimates of the maximum stress intensity factor. In certain circumstances this might give rise to concern.

REFERENCES

1. ASME Boiler & Pressure Vessel Code, Section XI, 1977, Rules for in-service inspection of nuclear power plant components.
2. Isida, M., Tsuru, H. & Noguchi, H., An analysis for three-dimensional cracks. *Fatigue Fract. Engng Mater. Struct.*, 1994, **17**, 737–749.
3. Noguchi, H. & Smith, R. A., An analysis of a

semi-infinite solid with three dimensional cracks. *Engng Fract. Mech.*, 1995, **52**, 1–14.
4. Nisitani, H. & Murakami, Y., Stress intensity factors of an elliptical crack or a semi-elliptical crack subject to tension. *Int. J. Fract.*, 1974, **10**, 353–368.
5. Mindlin, R. D., Force at a point in the interior of a semi-infinite solid. *Physics*, 1936, **7**, 195–202.
6. Mayrhofer, K. & Fischer, F. D., The stress-intensity factor distribution for an inclined elliptically shaped crack embedded near the surface of a halfspace—a solution for 3-D fatigue analysis. In *Proc. 5th Int. Conf. on Numerical Methods in Fracture Mechanics*, ed. A. R. Luxmore and D. R. J. Owen. Pineridge Press, Swansea, 1990, pp. 657–668.
7. Shah, R. C. & Kobayashi, A. S., *ASTM STP*, 1972, **513**, 3.
8. Isida, M., Hirota, K., Noguchi, H. & Yoshida, T., Two parallel elliptical cracks in an infinite solid subjected to tension. *Int. J. Fract.*, 1985, **27**, 31–48.
9. Newman, J. C. & Raju, I. S., An empirical stress intensity factor equation for the surface crack. *Engng Fract. Mech.*, 1981, **15**, 185–192.
10. Gilchrist, M. D., Chipalo, M. I. & Smith, R. A., Shape development of surface defects in tension fatigued finite thickness plates. *Int. J. Pres. Ves. & Piping*, 1992, **49**, 121–137.

APPENDIX

Tables A1–A3 contain numerical values for the normalised stress intensity factor around the whole of the crack front as calculated by the modified body force method.

Crack A—Elliptical crack with major axis parallel to the surface of the solid

Variation of $\frac{K_0}{\sigma_0\sqrt{\pi b}}$ *with the distance of the center of the crack from the surface of the solid.*

$b/a = 0{\cdot}5$, $\nu = 0{\cdot}3$, *loading = tension.*

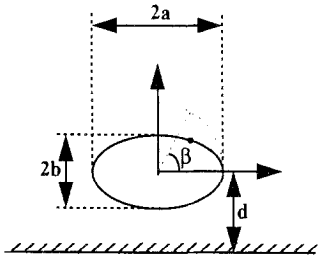

Table A1. Normalised stress intensity factors around the whole of the crack front for crack type A

d/b	Position on periphery of defect, β													Maximum stress intensity factor	
↓	0°	30°	60°	90°	120°	150°	180°	210°	240°	270°	300°	330°	360°	β	$\frac{K_1}{\sigma_0\sqrt{\pi b}}$
1·0	0·645	0·733	0·858	0·907	0·859	0·733	0·645	0·786	1·132	2·352	1·133	0·785	0·645	270°	2·352
1·05	0·634	0·722	0·845	0·892	0·845	0·722	0·634	0·763	1·036	1·373	1·037	0·764	0·634	270°	1·373
1·1	0·628	0·716	0·837	0·883	0·837	0·716	0·628	0·750	0·983	1·189	0·983	0·750	0·628	270°	1·189
1·2	0·619	0·707	0·826	0·871	0·826	0·707	0·619	0·731	0·919	1·040	0·920	0·731	0·619	270°	1·040
1·3	0·612	0·700	0·818	0·862	0·818	0·700	0·612	0·719	0·883	0·972	0·883	0·719	0·612	270°	0·972
1·4	0·607	0·695	0·812	0·856	0·812	0·696	0·607	0·709	0·860	0·933	0·860	0·710	0·607	270°	0·933
1·6	0·601	0·689	0·804	0·847	0·804	0·689	0·601	0·698	0·832	0·890	0·832	0·698	0·601	270°	0·890
1·8	0·596	0·684	0·799	0·842	0·799	0·685	0·596	0·690	0·816	0·868	0·816	0·691	0·596	270°	0·868
2·0	0·594	0·681	0·796	0·838	0·796	0·682	0·594	0·686	0·807	0·855	0·807	0·686	0·594	270°	0·855
∞	0·584	0·671	0·784	0·826	0·784	0·672	0·584	0·672	0·784	0·826	0·784	0·672	0·584	90, 270°	0·826

Crack B—Elliptical crack with major axis at an angle to the surface of the solid

Variation of $\frac{K_1}{\sigma_0\sqrt{\pi b}}$ *with rotation angle,* α, *of the major axis.*

$b/a = 0{\cdot}5$, $d/b = 1{\cdot}8$, $\nu = 0{\cdot}3$, *loading = tension.*

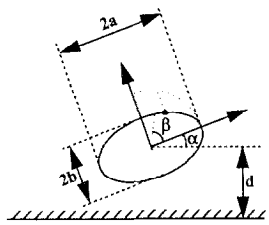

Table A2. Normalised stress intensity factors around the whole of the crack front for crack type B

α	Position on periphery of defect, β													Maximum stress intensity factor	
↓	0°	30°	60°	90°	120°	150°	180°	210°	240°	270°	300°	330°	360°	β	$\frac{K_1}{\sigma_0\sqrt{\pi b}}$
0°	0·596	0·684	0·799	0·842	0·799	0·685	0·597	0·691	0·816	0·868	0·817	0·690	0·596	270°	0·868
5°	0·595	0·683	0·798	0·842	0·800	0·686	0·598	0·693	0·820	0·868	0·814	0·689	0·595	269°	0·868
10°	0·594	0·683	0·798	0·842	0·801	0·687	0·600	0·696	0·824	0·867	0·811	0·687	0·594	267°	0·868
20°	0·593	0·681	0·797	0·843	0·804	0·692	0·606	0·705	0·833	0·867	0·808	0·685	0·593	265°	0·868
25°	0·592	0·681	0·797	0·843	0·806	0·695	0·608	0·712	0·838	0·867	0·806	0·683	0·592	263°	0·869
30°	0·592	0·680	0·797	0·844	0·808	0·699	0·615	0·721	0·845	0·866	0·805	0·683	0·592	261°	0·870
35°	0·591	0·680	0·797	0·845	0·810	0·704	0·623	0·733	0·851	0·866	0·804	0·682	0·592	260°	0·871
40°	0·591	0·680	0·797	0·846	0·813	0·710	0·633	0·750	0·858	0·865	0·803	0·682	0·591	257°	0·871
45°	0·591	0·680	0·797	0·847	0·817	0·718	0·648	0·774	0·864	0·865	0·802	0·681	0·591	255°	0·873
50°	0·590	0·679	0·797	0·848	0·821	0·730	0·673	0·811	0·870	0·865	0·802	0·681	0·591	251°	0·875
55°	0·590	0·679	0·797	0·849	0·827	0·746	0·718	0·870	0·878	0·865	0·801	0·680	0·590	240°	0·878

Crack C—Elliptical crack with minor axis at an angle to the surface of the solid

Variation of $\frac{K_I}{\sigma_0\sqrt{\pi b}}$ *with rotation angle,* α*, of the minor axis.*

$b/a = 1{\cdot}5$, $d/b = 1{\cdot}0$, $\nu = 0{\cdot}3$, *loading = tension.*

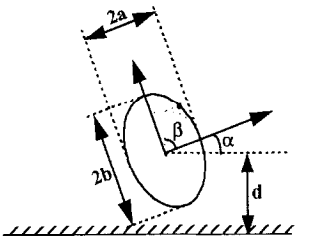

Table A3. Normalised stress intensity factors around the whole of the crack front for crack type C

α	Position on periphery of defect, β													Maximum stress intensity factor	
↓	0°	30°	60°	90°	120°	150°	180°	210°	240°	270°	300°	330°	360°	β	$\frac{K_I}{\sigma_0\sqrt{\pi b}}$
0°	0·644	0·609	0·549	0·512	0·549	0·609	0·644	0·651	0·674	1·030	0·674	0·651	0·644	271°	1·031
10°	0·642	0·608	0·549	0·512	0·549	0·610	0·647	0·659	0·697	0·798	0·640	0·642	0·642	264°	0·817
20°	0·639	0·608	0·549	0·512	0·549	0·611	0·649	0·665	0·697	0·658	0·612	0·633	0·639	251°	0·709
30°	0·637	0·607	0·548	0·512	0·550	0·612	0·652	0·668	0·667	0·597	0·592	0·626	0·637	228°	0·672
40°	0·635	0·607	0·549	0·512	0·551	0·614	0·655	0·667	0·633	0·565	0·578	0·621	0·635	207°	0·668
50°	0·633	0·606	0·549	0·513	0·552	0·616	0·658	0·663	0·606	0·546	0·569	0·616	0·633	200°	0·667
60°	0·632	0·606	0·549	0·514	0·553	0·618	0·660	0·656	0·588	0·534	0·562	0·613	0·632	194°	0·666
70°	0·631	0·607	0·550	0·515	0·555	0·621	0·663	0·647	0·575	0·527	0·558	0·611	0·631	189°	0·666
80°	0·631	0·607	0·551	0·516	0·558	0·626	0·665	0·639	0·567	0·522	0·555	0·609	0·631	184°	0·665
90°	0·631	0·608	0·553	0·519	0·562	0·632	0·665	0·632	0·561	0·519	0·552	0·608	0·631	180°	0·665